Volume 1 | Number 1 | Jan 2013 | Pages 1–100

ChemComm

Chemical Communications
www.rsc.org/chemcomm

ROYAL SOCIETY
OF CHEMISTRY

This is an *Accepted Manuscript*, which has been through the Royal Society of Chemistry peer review process and has been accepted for publication.

Accepted Manuscripts are published online shortly after acceptance, before technical editing, formatting and proof reading. Using this free service, authors can make their results available to the community, in citable form, before we publish the edited article. We will replace this *Accepted Manuscript* with the edited and formatted *Advance Article* as soon as it is available.

You can find more information about *Accepted Manuscripts* in the **Information for Authors**.

Please note that technical editing may introduce minor changes to the text and/or graphics, which may alter content. The journal's standard **Terms & Conditions** and the **Ethical guidelines** still apply. In no event shall the Royal Society of Chemistry be held responsible for any errors or omissions in this *Accepted Manuscript* or any consequences arising from the use of any information it contains.

ROYAL SOCIETY
OF CHEMISTRY

www.rsc.org/chemcomm

ChemComm

COMMUNICATION

Growth rates and water stability of 2D boronate ester covalent organic frameworks

Brian J. Smith, Nicky Hwang, Anton D. Chavez, Jennifer L. Novotney, and William R. Dichtel*

We examine the growth rates, activation energies, and hydrolytic stability of multiple 2D boronate ester covalent organic frameworks by turbidity measurements, observing a 200-fold range in stability. The rate-determining step in boronate ester 2D COF growth is not in-solution condensation, but rather interlayer polymer stacking through a nucleation-elongation process.

Covalent organic frameworks (COFs)[1–6] are an emerging class of crystalline, porous, multi-dimensional polymers with promise for applications in gas storage,[7,8] catalysis,[9–12] and energy storage and conversion devices.[13–17] An attractive feature of COFs is their designable crystalline structures, which are derived from the shape of the monomers and orientation of their reactive groups. However, several fundamental challenges continue to hinder COFs from realizing their full potential. COFs almost always form small crystalline domains (~30 nm), which ultimately aggregate into insoluble μm-sized polycrystalline particles. There have been no reports to date of a 2D COF single crystal and only one report of 3D systems isolated as single crystals.[18] Control of crystallite size (to provide either dispersible nanoparticles or macroscopic crystals) and exterior surface chemistry are both important milestones in COF chemistry that are so far lacking. Furthermore, COF synthesis remains highly empirical. Despite their modular design, optimal growth conditions for one network often do not translate to others. To enhance the modularity of COF synthesis and improve their long-range order, it is desirable to establish the sensitivity of COF synthesis and stability as a function of monomer structure. A greater understanding of COF formation will help to identify the source of these synthetic limitations and provide a rational approach for the development of the next generation of frameworks.

Department of Chemistry and Chemical Biology, Cornell University, Baker Laboratory, Ithaca, New York, 14853-1301. E-mail: wdichtel@cornell.edu
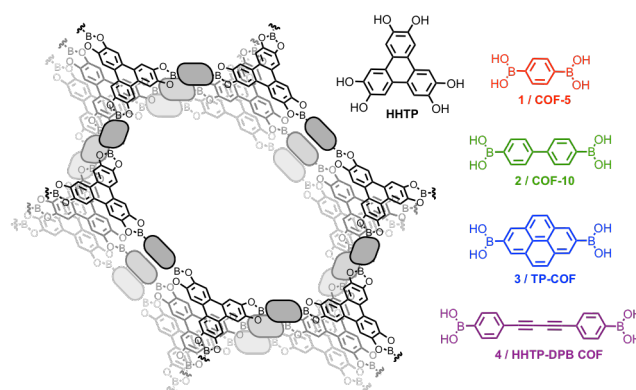
Scheme 1. Bis-boronic acid monomers (xBBA) and the corresponding HHTP-ester COF systems

We recently reported the first mechanistic study of COF growth.[19] The prototypical boronate ester framework, COF-5, precipitates within minutes when prepared from homogeneous conditions, enabling quantitative *in-situ* measurement of the COF formation rate. In contrast to the stochastic nature of small molecule crystallization, 2D boronate ester COF precipitation is highly reproducible. Turbidity measurements provide an experimental probe of the growth kinetics, allowing for modification of concentration, temperature, and additives to provide mechanistic insight. The complex rate law and irreversible nature of COF precipitation, both of which were contrary to common assumptions within the field, suggested that the stacking of the 2D polymers influences the rate of COF formation. Here we test this hypothesis by examining a series of 2D boronate ester COFs, synthesized under fully homogeneous conditions from 2,3,6,7,10,11-hexahydroxytriphenylene (HHTP) and various bis-boronic acid (xBBA) monomers (Scheme 1). COF-5,[20] COF-10,[21] TP-COF,[22] and HHTP-DPB COF,[23] are synthesized from HHTP and **1**, **2**, **3**, and **4**, respectively, systematically varying the monomer length and aromatic domain size. The COF growth

rate increases with enhanced van der Waals surface of the linker, despite minimal differences in the inherent rate of boronate ester formation, implicating a 2D nucleation-elongation growth mechanism.

In order to study comparable growth rates for each 2D COF, we developed homogeneous starting conditions for HHTP and xBBA monomers. Due to the low solubility of some xBBA species, the boronic acid suspensions were initially heated for 3 min in the absence of HHTP to fully dissolve the monomers (4:1 dioxane:mesitylene, 10 eq MeOH relative to xBBA), which remain in solution upon cooling to room temperature. The addition of HHTP and heating of these solutions to 90 °C yields COF powder precipitate within minutes for all four frameworks. The crystallinity of the filtered precipitates was confirmed by powder X-ray diffraction, with comparable crystallite sizes for the four systems examined (see Figures S1-S4). In the case of HHTP-DPB COF, activation by supercritical CO_2 provided enhanced X-ray scattering. For all systems, no evidence of co-crystallized monomers was observed in the final products by PXRD. The BET surface areas, determined from N_2 adsorption experiments, were comparable or better than the previously reported literature values. Most notably, the surface area obtained for HHTP-DPB COF is *ca.* 2400 m^2/g, which is more than double the value obtained under our previously reported conditions and approaches its Connolly surface area of 2650 m^2/g. We attribute this improvement to the absence of insoluble monomers contaminating the COF sample, greatly simplifying its activation using supercritical CO_2. Overall, initially homogeneous growth conditions are broadly applicable across several 2D COFs and yield samples of equal or superior average crystallite size and surface area.

The rates of COF formation were characterized by optical turbidity measurements. The initially homogeneous solutions were monitored at 1310 nm, where light absorption by the solvent and monomers is minimized. As the COF powder precipitates, the aggregated material scatters light, decreasing the measured transmission of the sample. This turbidity was calibrated with suspensions of pre-formed COF material to determine the percent yield of COF formation as a function of time (Figure 1). All four COF polymerizations exhibit a fully soluble induction period, followed by a rapid increase in turbidity associated with COF precipitation. TP-COF, formed from pyrene-based **3** and HHTP, has both the shortest lag period and the fastest initial rate of COF formation, nearly 20 % per minute. The rate of TP-COF formation is 35 times that of HHTP-DPB COF, which is its structural isomer. Generally, the rate of COF formation decreases with larger pore size and the corresponding higher fraction of empty space per unit cell. However, intramolecular interactions also play a strong role: the COF growth observed with pyrene-based **3** is over four times faster than bisphenyl-based **2**, despite nearly identical pore sizes. We attribute this phenomenon to the larger van der Waals surface area and forced planarity of **3**, which facilitate the crystallization of the 2D layered structure.

The four COFs were polymerized at different temperatures to determine the overall activation energies for the formation of each network. In all cases, lower temperatures slowed the rate of COF formation, and each COF exhibited a well-behaved Arrhenius temperature dependence (see Figures S13-S16). Over the temperatures examined, COF-5 and COF-10 have similar activation energies of 22–23 kcal/mol, while the activation energy for HHTP-DPB COF is higher, between 26–35 kcal/mol (Table 1). In contrast, TP-COF formation is much less sensitive to reaction temperature, with an activation energy of only 12
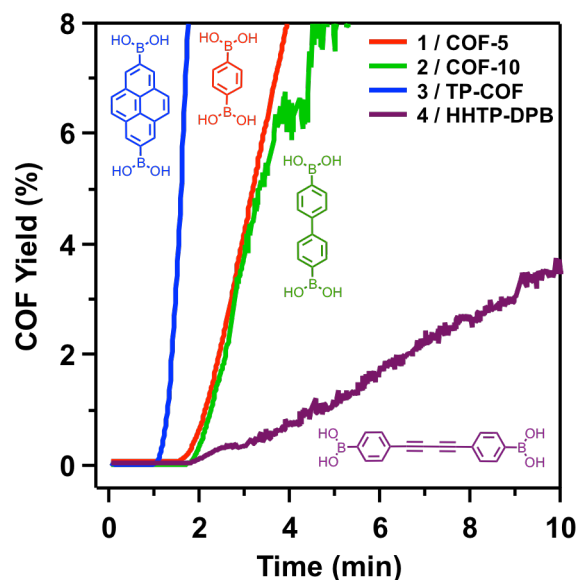
Fig 1. Percent Yield vs time for boronate ester COFs synthesized from homogeneous conditions (10 mM HHTP, 1.5 equiv. xBBA, 15 equiv. MeOH, 4:1 dioxane:mesitylene, 90˚C).

Table 1. Relative rates of formation and activation energies of HHTP-xBBA COFs

xBBA	COF	Relative Growth Rate (90˚C)	$E_{a\ COF}$ (kcal/mol)
1	COF-5	1	23 ± 1
2	COF-10	0.98	21 ± 1
3	TP-COF	4.6	12 ± 1
4	HHTP-DPB COF	0.13	31 ± 5

kcal/mol. This 10 kcal/mol difference in energy from the other boronate ester systems is consistent with the rapid TP-COF formation and shorter lag period observed, and it illustrates the large effect of the linker identity on the rate of growth.

To further probe the cause of the vastly different activation energies of TP-COF, we examined the formation of molecular boronate esters of **1** and **3** under similar conditions. **1** and **3** were reacted with 4-*tert*-butylcatechol (TCAT) at 60 °C, and boronate ester formation was monitored as a function of time by ^{1}H NMR spectroscopy (Figure 2). TCAT is an ideal substrate for these studies because its *tert*-butyl moiety both solubilizes the mono- and di-boronate ester products and provides a clear spectroscopic handle for the reaction progress. For both **1** and **3**, using an initial 1:1 [catechol]:[boronic acid] ratio, boronate ester formation is observed within minutes at 60 °C at comparable rates. This identical reaction progress is in sharp contrast to the corresponding COFs synthesized under identical conditions; at 10 minutes, approximately 10% TP-COF forms, compared to <1% COF-5. The TCAT boronate esters approach equilibrium at ~30% conversion after 10 minutes, suggesting that COF precipitation begins at low total conversions of starting materials. COF growth is more difficult to monitor directly by NMR spectroscopy than these model reactions because of the large number of overlapping

A ... TCAT ... + 4 H$_2$O

B ... **C**
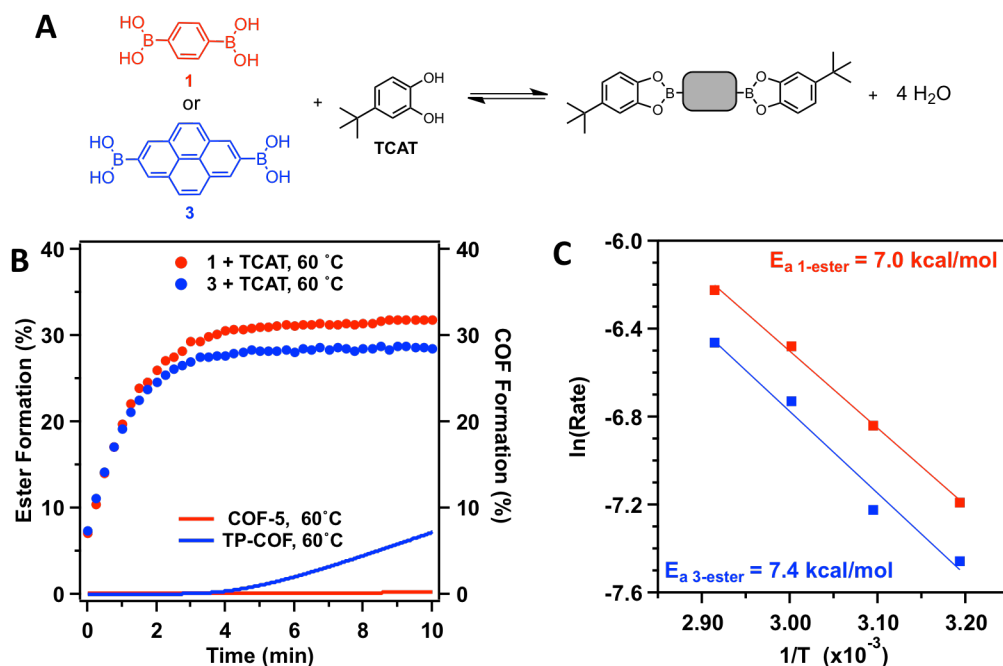
Fig 2. (A) Model homogeneous reaction (12 mM xBBA, 2 equiv. TCAT, 10 equiv. MeOH, 4:1 dioxane:mesitylene). (B) Boronate ester formation monitored by NMR at 60 °C, contrasted with COF growth under similar conditions (8mM HHTP, 1.5 equiv. xBBA, 15 equiv. MeOH). (C) Arrhenius plot calculating activation energies for boronate ester formation from 6:1 TCAT:xBBA conditions.

resonances of many possible boronate ester products. Nevertheless, NMR spectroscopy of the early stages of TP-COF polymerization indicated similarly low amounts of boronate ester formation at the onset of COF precipitation (see Figure S19). This precipitation of appreciable TP-COF at a low conversion to boronate esters is inconsistent with a polycondensation process. To reliably quantify the initial rate of boronate ester formation at various temperatures, excess TCAT (3:1 [catechol]:[boronic acid]) was used (see Figures S17-S18). The activation energies for boronate ester formation are similar for both **1** and **3**, *ca.* 7 kcal/mol, regardless of xBBA identity. This value is significantly less than the COF formation activation energies observed and further indicates that initial ester formation is not the rate determining process for these 2D COFs.

Together these results provide insight into the growth mechanism and rate determining process of COF formation. The insensitivity of boronate ester formation to xBBA identity suggests a rapid esterification pre-equilibrium prior to COF precipitation. The strong COF rate dependence on xBBA identity must therefore arise from a subsequent process. This conclusion is consistent with the observation that COF growth activation energies (12–31 kcal/mol) are significantly higher than those of small-molecule boronate ester formation (~7 kcal/mol). These results are also consistent with our observation of a complex rate expression for COF-5 growth, which is not explained by a simple boronate ester equilibrium.[19] Increasing linker length, from phenyl-based **1** to diphenylbutadiyne-based **4**, generally decreases the rate of COF formation. This is potentially due to the increasing pore sizes, which translate to a higher percentage of void space per unit cell, decreasing the interlayer attraction. However, the large difference in rate between pyrene-based **3** and bisphenyl-based **2** shows that pore size is not the only contributing factor. The van der Waals interactions of the large aromatic systems of

pyrene stabilize the polymer stacking intermediate, reflected in the appreciably lower activation energy. The four-fold rate increase from COF-5 to TP-COF suggests that the accelerating effect of the larger aromatic domains outweighs any rate decrease effect from the increasing pore size. Overall, we conclude that interlayer stacking of the 2D polymers is the rate-determining step, and the stronger intermolecular attraction of the pyrene moiety accelerates the COF formation. In contrast, systems with weaker intermolecular attraction exhibit longer
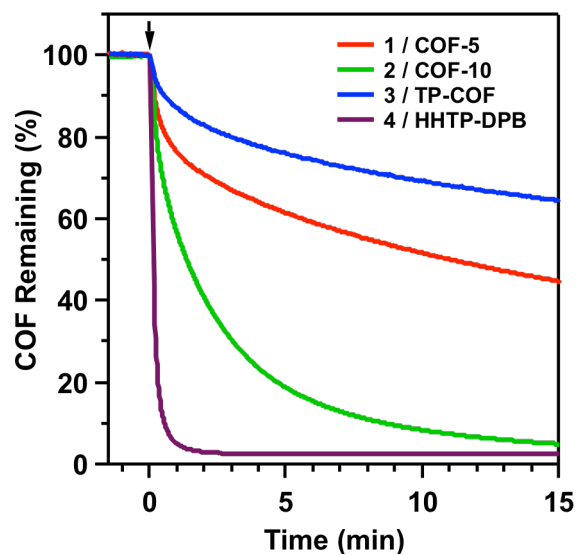
Fig 3. Hydrolytic digestion of COF suspensions at 25°C, monitored by turbidity. Water is added at *t* = 0 min (final [H$_2$O] = 0.7M in 4:1 dioxane:mesitylene, ~700 equiv. relative to HHTP)

periods in the solvated form. Whereas a simple polycondensation polymerization would only yield appreciable polymer at high conversions of monomer, TP-COF precipitates at times corresponding to < 50 % conversion of starting materials. These observations are more consistent with a nucleation-elongation type mechanism,[24] in which a 2D polymer templates the growth of a subsequent COF layer.

We postulated that the effect of increased van der Waals surface areas on COF formation would also be apparent in the hydrolytic stability of the isolated COF. Previous studies have shown that the water stability of boronate ester COFs can be increased by the addition of small quantities of pyridine or the modification of xBBA linkers with alkyl chains.[25–27] However, limited kinetic data could be determined for rapidly soluble systems. We monitored the digestion of COFs by tracking decreased suspension turbidity upon water addition, in a manner similar to the growth rate observation. This method provides a simple, rapid tool to quantify dissolution rates (Figure 3). Suspensions of each COF (0.5 mg/mL) in 4:1 dioxane:mesitylene were prepared at room temperature, which produce stable suspensions upon stirring. Excess H_2O (0.7 M final, ~700 equiv. relative to HHTP) was added, after which the turbidity was continuously monitored. In all cases, COF dissolution was observed immediately following H_2O addition, albeit at different rates. HHTP-DPB COF dissolves fastest, with 50% dissolution within 11 seconds and over 90% dissolution within the first minute. In contrast, its geometric isomer TP-COF displays a much greater hydrolytic stability, requiring 40 minutes for 50% dissolution, a >200-fold increase in stability. The trends are consistent with the relative growth rates, in that the more rapidly synthesized COFs also demonstrated greater water stability. Dissolution rates increase with larger pore sizes, at otherwise comparable intermolecular attraction. However, the drastic rate difference between TP-COF and COF-10 dissolution again indicates that pore size is not the only controlling factor. We conclude that the increased stability of the stacked pyrene-based **3** slows conversion to the boronic acid species by increasing the energy barrier to monomer release or interlayer exfoliation. This is consistent with previous theoretical work which predicts a greater intermolecular attraction in TP-COF over HHTP-DPB COF.[28] Future development of more hydrolytically stable 2D COFs should consider not only the linkage chemistry, but also the intermolecular attraction of the linker moieties.

In conclusion, four different 2D COFs were synthesized from fully homogeneous starting conditions, which provided samples of equal or better quality to previous literature reports. Measurement of the solution turbidity provides the first quantitative comparison of the growth rates of COFs of similar bonding and topology. COF formation rates depend on both pore size and the inter-layer attractive forces, and interlayer polymer stacking is the likely rate determining process. Increased aromatic domains yield greater 2D intermolecular attraction and a drastic increase in hydrolytic stability. In the design of next generation COF materials, the linker identity is an essential consideration, and systems with higher degrees of interlayer attraction may be targeted to maximize overall stability.

Acknowledgements

Notes and references

1 S.-Y. Ding and W. Wang, *Chem. Soc. Rev.*, 2012, **42**, 548–568.
2 X. Feng, X. Ding and D. Jiang, *Chem. Soc. Rev.*, 2012, **41**, 6010–6022.
3 J. W. Colson and W. R. Dichtel, *Nat. Chem.*, 2013, **5**, 453–465.
4 K. T. Jackson, T. E. Reich and H. M. El-Kaderi, *Chem. Commun.*, 2012, **48**, 8823–8825.
5 R. W. Tilford, S. J. Mugavero, P. J. Pellechia and J. J. Lavigne, *Adv. Mater.*, 2008, **20**, 2741–2746.
6 R. W. Tilford, W. R. Gemmill, H.-C. zur Loye and J. J. Lavigne, *Chem. Mater.*, 2006, **18**, 5296–5301.
7 M. G. Rabbani, A. K. Sekizkardes, Z. Kahveci, T. E. Reich, R. Ding and H. M. El-Kaderi, *Chem. – Eur. J.*, 2013, **19**, 3324–3328.
8 C. J. Doonan, D. J. Tranchemontagne, T. G. Glover, J. R. Hunt and O. M. Yaghi, *Nat. Chem.*, 2010, **2**, 235–238.
9 H. Xu, X. Chen, J. Gao, J. Lin, M. Addicoat, S. Irle and D. Jiang, *Chem. Commun.*, 2014, **50**, 1292–1294.
10 Q. Fang, S. Gu, J. Zheng, Z. Zhuang, S. Qiu and Y. Yan, *Angew. Chem. Int. Ed.*, 2014, **53**, 2878–2882.
11 D. B. Shinde, S. Kandambeth, P. Pachfule, R. R. Kumar and R. Banerjee, *Chem. Commun.*, 2014, **51**, 310–313.
12 S.-Y. Ding, J. Gao, Q. Wang, Y. Zhang, W.-G. Song, C.-Y. Su and W. Wang, *J. Am. Chem. Soc.*, 2011, **133**, 19816–19822.
13 C. R. DeBlase, K. E. Silberstein, T.-T. Truong, H. D. Abruña and W. R. Dichtel, *J. Am. Chem. Soc.*, 2013, **135**, 16821–16824.
14 S. Chandra, T. Kundu, S. Kandambeth, R. BabaRao, Y. Marathe, S. M. Kunjir and R. Banerjee, *J. Am. Chem. Soc.*, 2014, **136**, 6570–6573.
15 J. Guo, Y. Xu, S. Jin, L. Chen, T. Kaji, Y. Honsho, M. A. Addicoat, J. Kim, A. Saeki, H. Ihee, S. Seki, S. Irle, M. Hiramoto, J. Gao and D. Jiang, *Nat. Commun.*, 2013, **4**.
16 C. R. DeBlase, K. Hernández-Burgos, K. E. Silberstein, G. G. Rodríguez-Calero, R. P. Bisbey, H. D. Abruña and W. R. Dichtel, *ACS Nano*, 2015, DOI:10.1021/acsnano.5b00184.
17 G. H. V. Bertrand, V. K. Michaelis, T.-C. Ong, R. G. Griffin and M. Dincă, *Proc. Natl. Acad. Sci.*, 2013, **110**, 4923–4928.
18 D. Beaudoin, T. Maris and J. D. Wuest, *Nat. Chem.*, 2013, **5**, 830–834.
19 B. J. Smith and W. R. Dichtel, *J. Am. Chem. Soc.*, 2014, **136**, 8783–8789.
20 A. P. Côté, A. I. Benin, N. W. Ockwig, M. O'Keeffe, A. J. Matzger and O. M. Yaghi, *Science*, 2005, **310**, 1166–1170.
21 A. P. Côté, H. M. El-Kaderi, H. Furukawa, J. R. Hunt and O. M. Yaghi, *J. Am. Chem. Soc.*, 2007, **129**, 12914–12915.
22 S. Wan, J. Guo, J. Kim, H. Ihee and D. Jiang, *Angew. Chem. Int. Ed.*, 2008, **47**, 8826–8830.
23 E. L. Spitler, B. T. Koo, J. L. Novotney, J. W. Colson, F. J. Uribe-Romo, G. D. Gutierrez, P. Clancy and W. R. Dichtel, *J. Am. Chem. Soc.*, 2011, **133**, 19416–19421.
24 D. Zhao and J. S. Moore, *Org. Biomol. Chem.*, 2003, **1**, 3471–3491.
25 Y. Du, K. Mao, P. Kamakoti, P. Ravikovitch, C. Paur, S. Cundy, Q. Li and D. Calabro, *Chem. Commun.*, 2012, **48**, 4606–4608.
26 Y. Du, K. Mao, P. Kamakoti, B. Wooler, S. Cundy, Q. Li, P. Ravikovitch and D. Calabro, *J. Mater. Chem. A*, 2013, **1**, 13171–13178.
27 L. M. Lanni, R. W. Tilford, M. Bharathy and J. J. Lavigne, *J. Am. Chem. Soc.*, 2011, **133**, 13975–13983.
28 B. T. Koo, W. R. Dichtel and P. Clancy, *J. Mater. Chem.*, 2012, **22**, 17460–17469.